nature photonics

ARTICLES

PUBLISHED ONLINE: 1 JUNE 2014 | DOI: 10.1038/NPHOTON.2014.114

Emitters of *N*-photon bundles

C. Sánchez Muñoz[1], E. del Valle[1], A. González Tudela[2], K. Müller[3,4], S. Lichtmannecker[3], M. Kaniber[3], C. Tejedor[1], J. J. Finley[3] and F. P. Laussy[1]*

Controlling the output of a light emitter is one of the basic tasks in photonics, with landmarks such as the development of the laser and single-photon sources. The ever growing range of quantum applications is making it increasingly important to diversify the available quantum sources. Here, we propose a cavity quantum electrodynamics scheme to realize emitters that release their energy in groups (or 'bundles') of *N* photons (where *N* is an integer). Close to 100% of two-photon emission and 90% of three-photon emission is shown to be within reach of state-of-the-art samples. The emission can be tuned with the system parameters so that the device behaves as a laser or as an *N*-photon gun. Here, we develop the theoretical formalism to characterize such emitters, with the bundle statistics arising as an extension of the fundamental correlation functions of quantum optics. These emitters will be useful for quantum information processing and for medical applications.

The photon is the building block of light. Every state of the electromagnetic field exists as a superposition of photons, even classical states, which are Poisson distributions. Particular combinations of photons—ranging from more stringent distributions to entangled superpositions—are required to power quantum technology. Cavity quantum electrodynamics (cQED)[1] is one flexible platform used to sculpt desired states of light. These laboratories of the extreme allow the interaction of light with matter to be controlled at the ultimate quantum limit. We show here how they can be used to realize a family of N-photon emitters—sources that release their energy exclusively in groups (or bundles) of N photons (where N is an integer)—in effect providing us with light composed of building blocks that are no longer single photons. This ability to replace the quantum of light with a bundle has unforeseeable consequences, both for applications and for fundamental physics. For instance, it renormalizes the link between the energy of the fundamental unit of excitation to its frequency via a magnified Planck constant, $E = Nh\nu$. The type of emission can be varied with the system parameters to realize both N-photon lasers and photon guns[2] at the N-photon level. Such highly non-classical emitters should find use in the development of new generations of light sources[3,4], the production of NOON states[5], for quantum lithography and metrology[6], and also for medical applications, allowing greater penetration lengths and increased resolution with minimum harm to tissue[7,8]. The recent demonstration that biological photoreceptors are sensitive to photon statistics[9] may also render such sources highly relevant for studies of biological photosystems and, potentially, of quantum biology[10].

Jaynes–Cummings to Mollow dynamics transition

Our scheme relies on the cQED paradigm of one two-level system within a cavity (Fig. 1). This can be realized in a wide range of physical systems, from atoms in optical cavities[11] to superconducting qubits in microwave resonators[12] and quantum dots in microcavities[13]. The dynamics is described by the Jaynes–Cummings Hamiltonian[14] $H_0 = \omega_a a^\dagger a + \omega_\sigma \sigma^\dagger \sigma + g(a^\dagger \sigma + \sigma^\dagger a)$, where a and σ are the second quantization lowering operator of the light field (boson statistics) and the quantum emitter (QE, two-level system), respectively, with corresponding free energies ω_a and ω_σ and coupling strength g. The configuration under study involves the resonant excitation of the QE[15–17] by an external laser, far in the dispersive regime within the cavity $\left(|\omega_a - \omega_\sigma| \gg g\sqrt{N+1}\right)$[18–20]. The energy structure of H_0 is presented in Fig. 2a, with the QE at $\Delta/g = -60$ ($\Delta = \omega_a - \omega_\sigma$), where the states are essentially the bare ones. A laser of frequency ω_L and pumping intensity Ω is included by adding $H_\Omega = \Omega(e^{-i\omega_L t}\sigma^\dagger + e^{i\omega_L t}\sigma)$ to H_0. We assume the rotating wave approximation, the validity of which is justified in Supplementary Section III. At pumping that is low enough not to distort the level structure one can selectively excite a state with N photon(s) in the cavity at the $(N+1)$th rung by adjusting the laser frequency to

$$\omega_N \approx \omega_a + \frac{\sqrt{4(N+1)g^2 + \Delta^2} - \Delta}{2(N+1)} \qquad (1)$$

where $N \in \mathbf{N}$ (ref. 21). This is shown in Fig. 2a for $N = 2$, corresponding to the excitation of the third rung, with a photon blockade[22,23] at all other rungs (above and below)[24,25]. The positions of the resonances are shown in Fig. 3b. In the absence of dissipation, exciting a resonance leads to the generation of an exotic brand of maximally entangled polaritons of the type $(|0g\rangle \pm |Ne\rangle)/\sqrt{2}$ rather than the usual case $(|0e\rangle + |1g\rangle)/\sqrt{2}$. The dynamics of the system for $N = 2$ is presented in Fig. 4a. Strikingly, full-amplitude Rabi oscillations between the $|0g\rangle$ and $|Ne\rangle$ states are observed. Further characterization of these remarkable quantum states is provided in Supplementary Section I. We now consider towards the configuration that will bring such resonances to fruition in terms of applications.

When increasing pumping, resonances in the amplitude of the Rabi oscillations persist, but are blueshifted due to the dressing of the states by the laser. The level structure becomes that of a dressed atom[26] strongly detuned from a cavity mode[27], bridging the Jaynes–Cummings dynamics with another fundamental model of light–matter interaction, namely the Mollow physics of resonance

[1]Condensed Matter Physics Center (IFIMAC), Departamento de Física Teórica de la Materia Condensada, Universidad Autónoma de Madrid, 28049 Madrid, Spain, [2]Max-Planck-Institut für Quantenoptik, Hans-Kopfermann-Strasse 1, 85748 Garching, Germany, [3]Walter Schottky Institut, Technische Universität München, Am Coulombwall 4, 85748 Garching, Germany, [4]E. L. Ginzton Laboratory, Stanford University, Stanford, California 94305, USA. *e-mail: fabrice.laussy@gmail.com

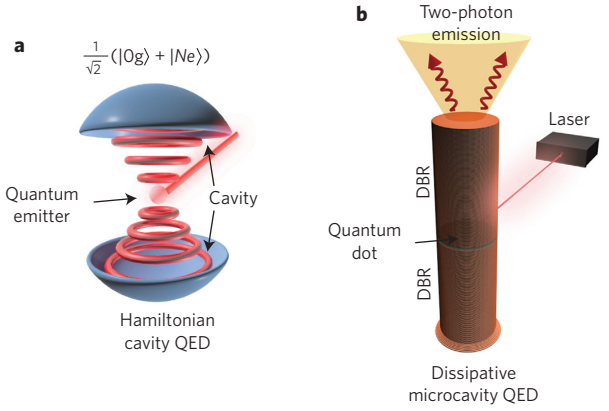

Figure 1 | Hamiltonian and dissipative cavity QED. a, cQED brings QED (the theory of light–matter interactions) under prolonged scrutiny at the level of a few photons and in the presence of a quantum emitter. An external laser can be applied to the emitter to drive its dynamics. We show how peculiar quantum superpositions can be realized and the emission subsequently forced to take place exclusively in bundles of N photons. **b**, A possible solid-state implementation of our proposal places a quantum dot in a micropillar. With excitation from the side with a conventional laser, one can collect, in the cavity, emission as the output from a quantum laser or a quantum gun, depending on the system parameters. DBR, distributed Bragg reflector.

fluorescence[28]. The strong coupling that was previously dominated by the interaction between the QE and a cavity photon and was probed by the laser is now dominated by the interaction of the QE with the laser photons and is probed by the cavity. This elegant transition between the two pillars of nonlinear quantum optics brings the resonances in equation (1) to the form

$$\omega_N(\Omega) \approx \omega_a + \frac{\sqrt{4(N^2-1)\Omega^2 + N^2\Delta^2} + \Delta}{N^2-1} \qquad (2)$$

Equation (2) is realized when the energy of N cavity photons matches the N-photon transition between the $|-\rangle$ and $|+\rangle$ levels of the dressed atom[29], as shown in Fig. 2b for $N=2$. In the indeterminate case $N=1$, equation (2) should be taken in the limit $N \to 1$, yielding $\omega_L = \omega_a - (2\Omega^2 + \Delta^2/2)/\Delta$ (in the dispersive regime, $\Delta \neq 0$).

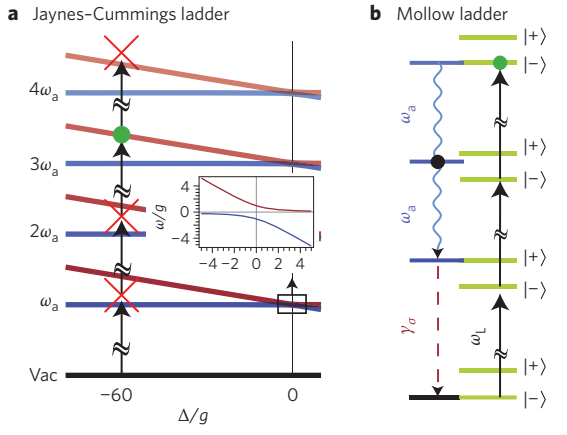

Figure 2 | Energy levels of the two limiting cases of excitation. a, In the low-excitation regime the Jaynes–Cummings ladder (anticrossing magnified in the inset) is probed by resonantly exciting a given rung of the ladder, with photon blockade at all others. **b**, In the high-excitation regime, the laser dresses the QE while the cavity Purcell-enhances an N-photon transition from $|-\rangle$ to $|+\rangle$ (here for $N=2$). A subsequent emission from the QE brings the system back to a $|-\rangle$ state.

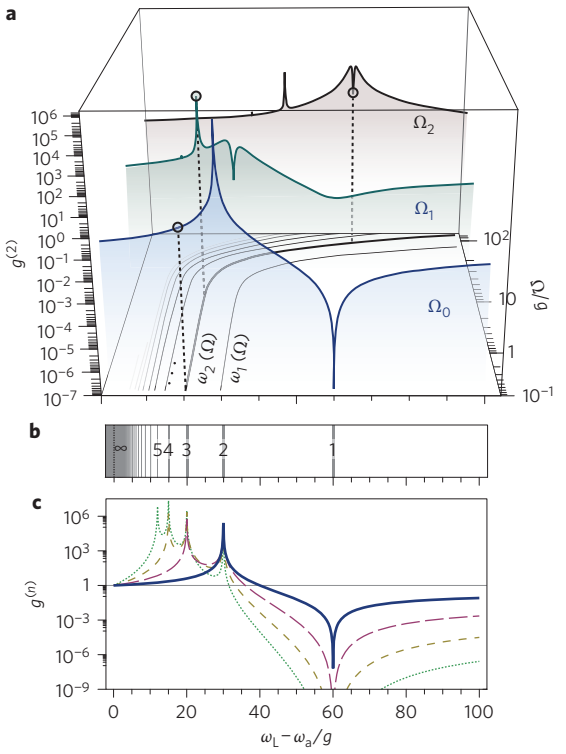

Figure 3 | Resonances in the photon-correlation functions. a, $g^{(2)}$ as a function of ω_L for pumping $\Omega_0 \approx 10^{-2}g$, $\Omega_1 \approx 4g$ and $\Omega_2 \approx 32g$. The resonances $\omega_N(\Omega)$ are shown in the plane (ω_L,Ω). Open circles are the projection of ω_2 on $g^{(2)}$. **b**, Resonant energies to excite the nth rung of the ladder. **c**, $g^{(n)}$ for $n=2$ (solid), 3 (long dash), 4 (short dash) and 5 (dotted) at vanishing pumping with n–1 bunching resonances matching those in **b**. $\Delta/g = -60$ in all panels.

All the dynamics discussed so far correspond to systems that are Hamiltonian in nature, such as atomic cQED realizations[30].

Dissipation as a trigger of quantum emission

Strong dissipation, as in semiconductor cQED, is not always detrimental to quantum effects[31,32]. Indeed, Purcell enhancement of the Hamiltonian resonances just described may give rise to giant photon correlations in the statistics of the field detected outside the cavity, instead of Rabi oscillations[33,34]. The corresponding zero-delay photon correlations[35] $g^{(n)} = \langle a^{\dagger n} a^n \rangle / \langle a^\dagger a \rangle^n$ are shown in the limit of vanishing pumping in Fig. 3c. An antibunching dip is observed for each $g^{(n)}$ when resonantly exciting the emitter, followed by a series of $n-1$ huge bunching peaks that match the resonances in equation (1), as plotted in Fig. 3b. In these calculations, the Hamiltonian has been supplemented with superoperators in the Lindblad form to describe dissipation of the cavity (respectively QE) at a rate γ_a (respectively γ_σ)[36] (see Methods). The parameters used are $\gamma_a/g = 0.1$ and $\gamma_\sigma/g = 0.01$. Details of the formalism, as well as its extension to describe decoherence, are given in Supplementary Section VI. As pumping is increased, resonances in $g^{(n)}$ shift along the curves $\omega_N(\Omega)$ in the (ω_L, Ω) space defined by equation (2). This is shown for $g^{(2)}$ in Fig. 3a for three values of pumping (for an animation see the Supplementary Movie), starting with $\Omega_0 = 10^{-1}g$, close to the vanishing pumping case shown in Fig. 3c. Following $g^{(2)}$ along the ω_2 resonance reveals that a new peak emerges out of a uniform background, reaching a maximum $g^{(2)} \approx 3{,}649$ at the pumping $\Omega_1 \approx 4g$ (middle trace) before a depletion of the resonance forms for higher pumping, reaching its minimum along ω_2 of $g^{(2)} \approx 17$ at $\Omega_2 \approx 32g$ (background trace). So far, we have therefore transferred some

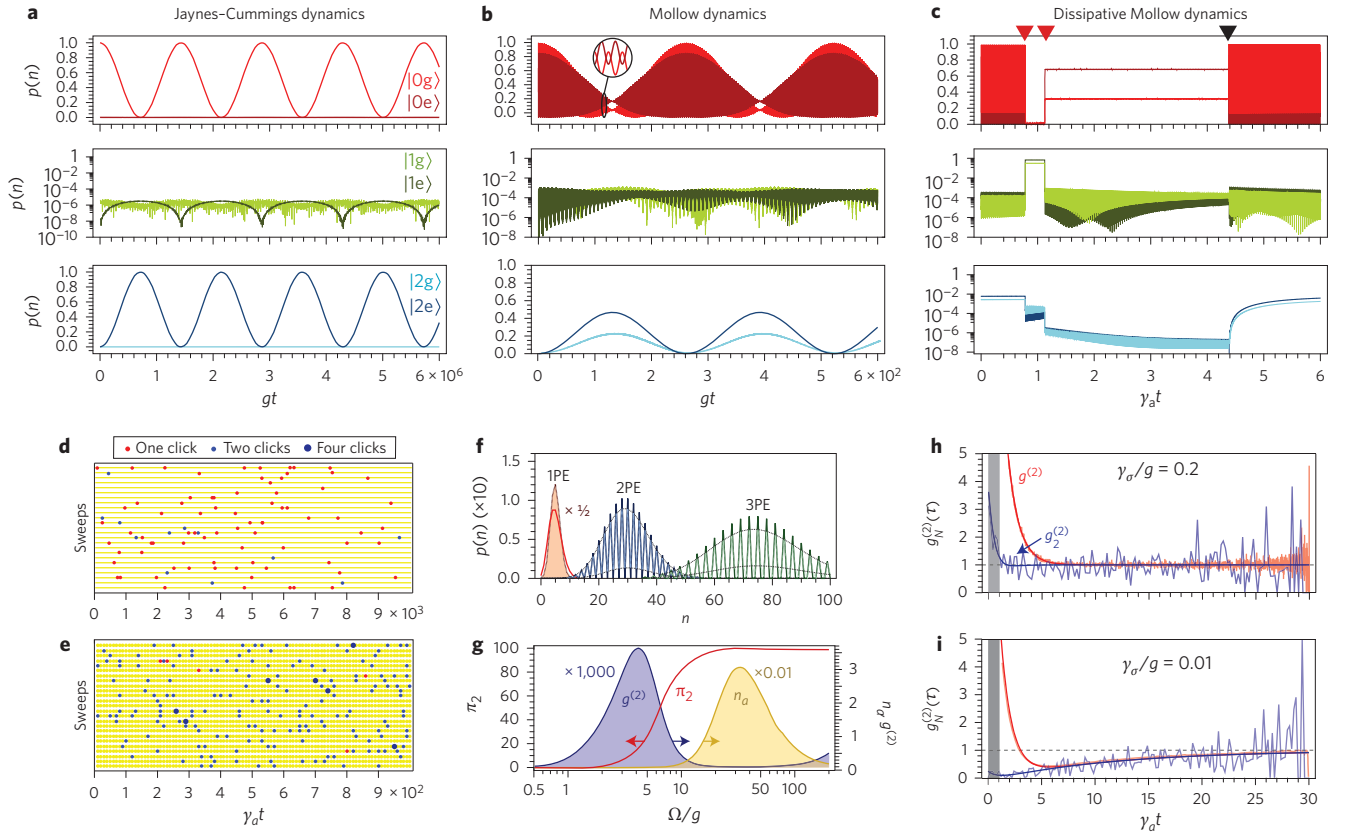

Figure 4 | Dynamics of the emission when probing the two-photon resonance in various regimes of excitation. a, Wavefunction evolution at the two-photon resonance pictured through the probability of the system to be in any of the states $|ng/e\rangle$. Hamiltonian evolution in the Jaynes–Cummings regime (low pumping). **b**, Hamiltonian evolution in the Mollow regime (high pumping). **c**, Quantum trajectory during two-photon emission in the same regime as in **b**, but in the presence of dissipation. **d**,**e**, Cavity-photon clicks as they would be recorded by a streak camera (25 sweeps shown) for pumping values Ω_1 (**d**) and Ω_2 (**e**) at $\omega_2(\Omega)$. In **d**, the emission is highly bunched, although it largely consists of single clicks ($g^{(2)} = 3{,}649$ and $\pi_2 = 16\%$). In **e**, $g^{(2)} = 17$ with $\pi_2 = 98.8\%$. **f**, Ideal *N*PE (*N*-photon emission) in thick lines and 99% *N*PE in translucent lines with an envelope to guide the eye. **g**, Pumping dependence of π_2 (left axis) and $g^{(2)}$ (right axis) (from 0 to 3,649) and n_a (from 0 to 0.03) following $\omega_2(\Omega)$. **h**,**i**, Second-order photon correlations at the $N = 1$ (red) and $N = 2$ (blue) level, from equation (6) (smooth curve) and from Monte Carlo clicks (data).

attributes of the remarkable quantum states produced by the cQED system to the outside world. We now proceed to show in which regimes and in which sense this transfer can actually be used for applications.

Strong correlations do not guarantee useful emission

The resonances in $g^{(n)}$ are indicative of strong correlations, but not in an intuitive way nor in a particularly useful one for applications. Indeed, $g^{(2)}$ (we discuss the case $n = 2$ with no loss of generality) is unbounded and cannot be interpreted in terms of the probability of two-photon emission. Other quantities to measure correlations, such as the differential correlation function[37] or the surge[38], present the same problem. To gain insights into the dissipative context, we turn to a quantum Monte Carlo approach[39], where one follows individual trajectories of the system and records photon clicks whenever the system undergoes a quantum jump. A tiny fraction of such a trajectory is presented in Fig. 4c (a larger fraction is provided in Supplementary Section II). This shows the probabilities of the system to be in the states $|ng/e\rangle$ for n up to 2 (probabilities in higher rungs are included in the numerical simulation).

Until time $t \approx 0.8$ (in units of $1/\gamma_a$), the QE essentially undergoes fast Rabi flopping (in an empty cavity) under the action of the laser, corresponding to the Mollow regime. At the same time, the driving of the third rung makes the probability of having two photons in the cavity sizable, as seen in the bottom panel of Fig. 4c, where the combined probability reaches over 1% (while the probability of having one photon is more than one order of magnitude smaller). This relatively high probability of the two-photon state, given the time available to realize it, eventually results in its occurrence. This causes the emission of a first cavity photon (indicated by a red triangle at the top of the figure) that collapses the wavefunction into the one-photon state, which is now the state with almost unit probability. The system is now expected to emit a second photon within the cavity lifetime (second red triangle in Fig. 4c). There is a jitter in the emission of the two-photon state due to the cavity, but this does not destroy their correlation. After the two-photon emission the system is left in a vacuum state but without Rabi flopping; this is restored after a direct emission from the QE (black triangle) and a two-photon state is again constructed, preparing for the next emission of a correlated photon pair. The system is then brought back to its starting point. Although one photon coming from the QE decay is emitted per two-photon emission cycle, it is at another frequency and with a different solid angle. The two-photon emission takes place through the cavity mode and is therefore unspoiled and strongly focused.

Figure 4d,e presents a series of detection events (such as would be recorded by a streak camera photodetector[40]) for the pumping values Ω_1 and Ω_2 of Fig. 3a at $\omega_2(\Omega)$. The horizontal axis represents time, and each point denotes a detection event as the detection spot is raster-scanned across the image. The strong bunching at Ω_1 in Fig. 3a conveys that the number of correlated two-photon events (blue points) in Fig. 4d is much larger than would be expected for

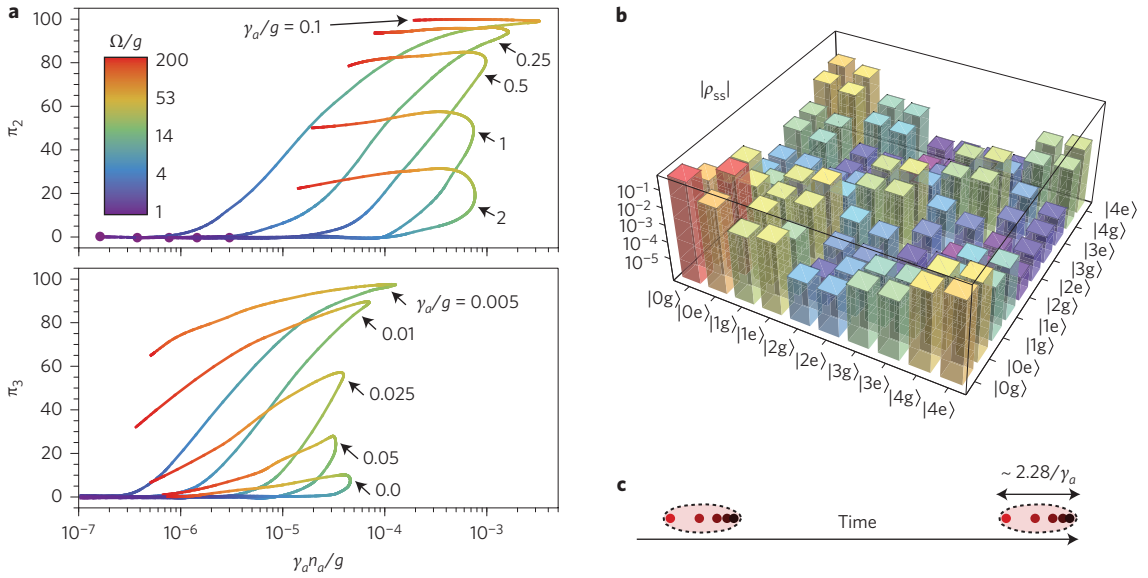

Figure 5 | Efficiency and characterization of *N*-photon emission for $2 \leq N \leq 5$ a, Figures of merit for two- and three-photon emission in the space of purity/emission intensity. Almost pure two- and three-photon emission can be achieved with state-of-the-art cQED samples: $\gamma_a/g = 0.01$ for π_2 and 0.001 for π_3. **b**, Full density matrix of the system in the regime of four-photon emission, showing the predominance of the vacuum and the strong coherence between the 2×2 sub-blocks of 0 and 4 photons and the $1/n$ cascade along the diagonal. **c**, Sketch of two five-photon bundles. Each bundle is composed of photons that pile up together ahead in time due to the mechanism of their production. This structure is not described by the state $|5\rangle$.

a coherent source. Nevertheless, the emission remains predominantly in terms of single photons (red points). Accordingly, although the resonances in the statistics are strong, they are not meaningful for applications. On the other hand, at Ω_2, when the $g^{(2)}$ resonance is depleted, the emission now consists almost exclusively of correlated photon pairs, as can be seen by the dominance of blue points in Fig. 4e.

Definition of purity of *N*-photon emission

Because the standard correlation functions $g^{(n)}$ do not correspond to actual N-photon emission, the problem arises of how to describe what is in fact the most important feature of such an emitter: the amount of N-photon emission. Photon counting[41–43] is a convenient way to do this in practical terms, as an ideal N-photon emitter never produces a number of photons that is not a multiple of N (ref. 44). We observe that for time windows T larger than the coherence time, counting of the photon bundles becomes Poisson distributed, as short time correlations are lost[45]. This distribution is shown in Fig. 4f for the cases of ideal two-photon (2PE) and three-photon (3PE) emission. However, a non-ideal N-photon emitter occasionally emits single photons that spoil these distributions. If bundle events are represented by the Poisson parameter λ_N and single events by λ_1, one finds (see Methods) that the distribution of counting n photons in time window T is given by

$$P_N(n) = e^{-(\lambda_1+\lambda_N)T} \sum_{k=0}^{n} \frac{n!(\lambda_1 T)^{n-Nk}(\lambda_N T)^k}{k!(n-Nk)!} \qquad (3)$$

When the suppression of photon emission that is not a multiple of N is efficient, these parameters are related to the cavity population n_a through $\lambda_N = \gamma_a n_a/N$. As the λ parameters are independent of the time window T, we can define the 'purity' of the N-photon emission π_N as

$$\pi_N = \lambda_N/(\lambda_1 + \lambda_N) \qquad (4)$$

This ratio represents the percentage of the emission that exists as N-photon bundles, which can now be contrasted with $g^{(N)}$, as shown in Fig. 4g for $N = 2$. Here we find the remarkable result that $g^{(2)}$, often described as the probability for two-photon emission, is in fact anticorrelated with π_2, the actual such probability: when $g^{(2)}$ reaches its maximum π_2 is starting to grow, and when π_2 is maximum $g^{(2)}$ is locally minimum, although still larger than one.

We characterize the efficiency of N-photon emission by plotting the purity and emission intensity together (Fig. 5a) for π_2 and π_3. Because N-photon emission is a $(N+1)$th-order process, it is more easily overcome by dissipation as N increases. Nevertheless, almost pure two-photon and three-photon emission is already feasible with state-of-the-art cQED systems. Indeed, ~85% of two-photon emission can already be obtained with current semiconductor samples ($\gamma_a/g \approx 0.5$, $g \approx 12$ GHz)[46,47] with a rate of over 1×10^7 counts per second, while circuit QED systems ($\gamma_a/g \approx 0.01$, $g \approx 50$ MHz)[48] can even reach ~90% of three-photon emission with a rate of 1×10^3 counts per second. N-photon emission takes place when the coupling is large enough for the cavity to stop acting as a mere filter and actually Purcell-enhance the corresponding multiphoton transitions[49]. These results are extremely robust against dephasing, thanks to the short time window in which a bundle is generated and emitted, as is shown in Supplementary Section VI.

Relation between the bundle and a Fock state

We have described the emission of our system in terms of bundles of photons, introducing a terminology that needs to be justified. In quantum theory, a state of the field with exactly N quanta of excitation is a Fock state $|N\rangle$, and it is natural to question whether our device is not precisely an 'emitter of Fock states $|N\rangle$'.

There are subtle links and departures between the two concepts. The Fock state $|N\rangle$ is a well-defined state that can be prepared and maintained exactly. It has no further structure and each of the N photons that compose it is fully indistinguishable from the others. The bundle, on the other hand, arises in a dynamical process of emission, describing the energy released from the cQED set-up to the outside world. The cavity itself is not in the Fock state $|N\rangle$ being, to begin with, in the vacuum most of the time; only in very short temporal windows does it undergo a cascade that sees the field transit through the various Fock states $|n\rangle$ in rapid succession, where $0 \leq n \leq N$ and for a time $1/(\gamma_a n)$ in each of them. Because the

system has a small probability of being in state $|N\rangle$ before the emission and a probability close to one of transiting through each of the intermediate states during the cascade, one obtains the steady-state probability

$$p(n) = \frac{n_a}{N}\frac{1}{n}, \quad \text{for } 1 \le n \le N \tag{5}$$

A snapshot of the full density matrix in the regime of four-photon emission is given in Fig. 5b. This shows the breakdown of the matrix into clusters of 2×2 blocks corresponding to the subspaces of the QE with n photons. The vacuum largely predominates (probabilities are shown in a logarithmic scale), followed by the blocks on the diagonal, which provide $p(n)$ as given by equation (5), and blocks of coherence between the various manifolds, which are small although non-zero, except the coherence elements $|0\mu\rangle\langle 4\nu|$ with $\mu,\nu \in \{g, e\}$, which are large. This confirms the direct manifestation, also in the dissipative regime, of the quantum superposition of the type $(|0g\rangle \pm |Ne\rangle)/\sqrt{2}$.

There remains a trace of this intracavity dynamics in the photodetection. The bundles are strongly correlated in two senses: (1) extrinsically, the emission occurs in groups of N photons, suppressing the release of packets with other numbers of photons; (2) intrinsically, with different time intervals separating successive photons, the first photon is more closely followed by the second one than the second is by the third, and so on until the last photon, which comes within $1/\gamma_a$ of the penultimate photon (Fig. 5c). Clearly, the bundle is a strongly correlated group of closely spaced photons and has a structure that is not described by the abstract object $|N\rangle$ alone. However, regardless of the internal structure of the bundle, it would appear as a Fock state in a measurement integrated over a small time window. Further discussion with the Wigner function can be found in Supplementary Section IV.

Regimes of *N*-photon emission: guns and lasers

Now that we have engineered N-photon emitters we have to ask the same questions as put by Glauber[35] at the dawn of quantum optics regarding the nature of quantum optical coherence for these sources. The answer is as simple as it is beautiful: N-photon emitters are the exact counterpart of conventional emitters, but the unit of emission—the photon—is replaced by a bundle of N photons. We now show that our class of emitters can operate in the same regimes as lasers or photon guns, but with bundles. To do so, we describe the statistics of the bundles when considered as single entities by introducing the generalized correlation functions $g_N^{(n)}$:

$$g_N^{(n)}(t_1,\ldots,t_n) = \frac{\langle \mathcal{T}_-\{\prod_{i=1}^n a^{\dagger N}(t_i)\}\mathcal{T}_+\{\prod_{i=1}^n a^N(t_i)\}\rangle}{\prod_{i=1}^n \langle a^{\dagger N}a^N\rangle(t_i)} \tag{6}$$

where $\mathcal{T}_\pm$ represents the time ordering operators. This upgrades the concept of the nth-order correlation function for isolated photons to bundles of N photons. The case $N = 1$ recovers the definition of the standard $g^{(n)}$, but for $N \ge 2$, normalization to the bundle density makes equation (6) essentially different from the standard correlation functions $g^{(n\times N)}$. Similarly to the single-photon case, the two-bundle statistics

$$g_N^{(2)}(\tau) = \frac{\langle a^{\dagger N}(0)a^{\dagger N}(\tau)a^N(\tau)a^N(0)\rangle}{\langle (a^{\dagger N}a^N)(0)\rangle\langle (a^{\dagger N}a^N)(\tau)\rangle} \tag{7}$$

is the most important. The validity of this definition for $g_2^{(2)}$ is confirmed in Fig. 4h,i, where it is plotted (smooth curve) together with direct coincidences between clicks from the Monte Carlo simulation (data). Such $g_2^{(2)}$ correlations can be measured directly thanks to recent developments in two-photon detection[50]. For the Monte Carlo computation, all events are considered as single photons for the standard $g^{(2)}$ calculation (red curve in Fig. 4h,i), and only two-photon events are considered as the basic unit of emission for $g_2^{(2)}$ (blue curve). Except in the small jitter window of width $1/\gamma_a$ in which they cannot be defined, photon pairs exhibit antibunching for long-lived QE, while they are Poisson-distributed for short-lived QE. In the latter case one can check that $g_2^{(3)}(\tau_1, \tau_2) = 1$ except for in the aforementioned jitter window (see Supplementary Section V). The emitter therefore behaves respectively as a two-photon gun and—according to Glauber[35]—as a laser, but at the two-photon level. The effect the QE lifetime has on the statistics of the bundles can be understood as a consequence of the key role the QE emission plays to restore the construction of an N-photon state. At the single-photon level, the standard $g^{(2)}(\tau)$ fails to capture this fundamental dynamics of emission. All this confirms the emergence of a new physics at the two-photon level. The same behaviours hold for higher N.

Methods

System dynamics. To describe dissipation in addition to the Hamiltonian dynamics, we resort to a master equation in the Lindblad form[36]:

$$\dot{\rho} = -i[H,\rho] + \left[\frac{\gamma_a}{2}\mathcal{L}_a + \frac{\gamma_\sigma}{2}\mathcal{L}_\sigma\right]\rho \tag{8}$$

expressed in terms of the Liouvillian super-operator $\mathcal{L}_c\rho = 2c\rho c^\dagger - c^{\mathrm{nA}}c\rho - \rho c^\dagger c$, where γ_a and γ_σ are the decay rates of the cavity and quantum emitter, respectively and $H = H_0 + H_\Omega$. By arranging the elements of the density matrix in a vectorial form, we can express this equation as $\dot{\vec{\rho}} = M\vec{\rho}$, from which the steady-state density matrix $\vec{\rho}_{ss}$ is obtained as the null space of the matrix M. A more general expression that takes into account additional dephasing terms is provided and investigated in Supplementary Section VI.

For photon-counting calculations, we solve the same problem using the Monte Carlo method of quantum trajectories, which allows the use of a wavefunction picture in a dissipative context. In this approach, one uses an evolution operator constructed with a non-Hermitian Hamiltonian $H_{\mathrm{eff}} = H - i\frac{\gamma_a}{2}a^\dagger a - i\frac{\gamma_\sigma}{2}\sigma^\dagger\sigma$, whose resulting dynamics can be interrupted in each time step δt by a quantum jump acting on the wavefunction as $c|\psi\rangle/\langle\psi|c^\dagger c|\psi\rangle$ ($c \in \{a, \sigma\}$) with probability $p_c = \delta t\ \gamma_c\ \langle\psi|c^\dagger c|\psi\rangle$. These jump events are then recorded as photon emissions coming from the cavity or the QE.

Photon-counting distribution for the imperfect *N*-photon emitter. In the limit in which the counting of N-photon bundles becomes Poisson distributed, the random variable X_N that counts them in a time window T follows the distribution $P(X_N = k) = \exp(-\lambda_N T)(\lambda_N T)^{k/N}/(k/N)!$ if k is a multiple of N and is zero otherwise, with a generating function $\Pi_{X_N}(s) = \langle s^{X_N}\rangle = e^{-\lambda_N(1-s^{1/N})}$. A non-ideal N-photon emitter also emits single photons that spoil these distributions. Photon counting then results from the sum of two random variables $X_1 + X_N$, where X_1 is a conventional Poisson process. The generating function of the imperfect N-photon emitter is $\Pi_{X_1+X_N} = \Pi_{X_1}\Pi_{X_N}$, where $\Pi_1 = e^{-\lambda_1(1-s)}$ is the generating function of a Poissonian distribution. The closed-form expression provided in the text is straightforwardly derived as $P_N(n) = \frac{1}{n!}\partial^n\Pi_{X_1+X_N}/\partial s^n|_{s=0}$.

Received 20 December 2013; accepted 23 April 2014; published online 1 June 2014

References

1. Haroche, S. Nobel lecture: Controlling photons in a box and exploring the quantum to classical boundary. *Rev. Mod. Phys.* **85,** 1083–1102 (2013).
2. Lounis, B. & Orrit, M. *Rep. Prog. Phys.* **68,** 1129 (2005).
3. Walther, H., Varcoe, B. T. H., Englert, B.-G. & Becker, T. Cavity quantum electrodynamics. *Rep. Prog. Phys.* **69,** 1325–1382 (2006).
4. O'Brien, J. L., Furusawa, A. & Vučkovic, J. Photonic quantum technologies. *Nature Photon.* **3,** 687–695 (2009).
5. Afek, I., Ambar, O. & Silberberg, Y. High-NOON states by mixing quantum and classical light. *Science* **328,** 879–881 (2010).
6. Giovannetti, V., Lloyd, S. & Maccone, L. Quantum-enhanced measurements: beating the standard quantum limit. *Science* **306,** 1330–1336 (2004).
7. Denk, W., Strickler, J. H. & Webb, W. W. Two-photon laser scanning fluorescence microscopy. *Science* **248,** 73–76 (1990).
8. Horton, N. *et al. In vivo* three-photon microscopy of subcortical structures within an intact mouse brain. *Nature Photon.* **7,** 205–209 (2013).
9. Sim, N., Cheng, M. F., Bessarab, D., Jones, C. M. & Krivitsky, L. A. Measurement of photon statistics with live photoreceptor cells. *Phys. Rev. Lett.* **109,** 113601 (2012).

10. Ball, P. Physics of life: the dawn of quantum biology. *Nature* **474,** 272–274 (2011).
11. Brune, M. *et al.* Quantum Rabi oscillation: a direct test of field quantization in a cavity. *Phys. Rev. Lett.* **76,** 1800–1803 (1996).
12. Fink, J. M. *et al.* Climbing the Jaynes–Cummings ladder and observing its $\sqrt{n}$ nonlinearity in a cavity QED system. *Nature* **454,** 315–318 (2008).
13. Kasprzak, J. *et al.* Up on the Jaynes–Cummings ladder of a quantum-dot/microcavity system. *Nature Mater.* **9,** 304–308 (2010).
14. Jaynes, E. T. & Cummings, F. W. Comparison of quantum and semiclassical radiation theory with application to the beam maser. *Proc. IEEE* **51,** 89–109 (1963).
15. Nguyen, H. S. *et al.* Ultra-coherent single photon source. *Appl. Phys. Lett.* **99,** 261904 (2011).
16. Matthiesen, C., Vamivakas, A. N. & Atatüre, M. Subnatural linewidth single photons from a quantum dot. *Phys. Rev. Lett.* **108,** 093602 (2012).
17. Jayakumar, H. *et al.* Deterministic photon pairs and coherent optical control of a single quantum dot. *Phys. Rev. Lett.* **110,** 135505 (2013).
18. Majumdar, A. *et al.* Linewidth broadening of a quantum dot coupled to an off-resonant cavity. *Phys. Rev. B* **82,** 045306 (2010).
19. Hughes, S. & Carmichael, H. J. Stationary inversion of a two level system coupled to an off-resonant cavity with strong dissipation. *Phys. Rev. Lett.* **107,** 193601 (2011).
20. Laussy, F. P., del Valle, E., Schrapp, M., Laucht, A. & Finley, J. J. Climbing the Jaynes–Cummings ladder by photon counting. *J. Nanophoton.* **6,** 061803 (2012).
21. Chough, Y.-T., Moon, H.-J., Nha, H. & An, K. Single-atom laser based on multiphoton resonances at far-off resonance in the Jaynes–Cummings ladder. *Phys. Rev. A* **63,** 013804 (2000).
22. Birnbaum, K. *et al.* Photon blockade in an optical cavity with one trapped atom. *Nature* **436,** 87–90 (2005).
23. Faraon, A. *et al.* Coherent generation of non-classical light on a chip via photon-induced tunnelling and blockade. *Nature Phys.* **4,** 859–863 (2008).
24. Schuster, I. *et al.* Nonlinear spectroscopy of photons bound to one atom. *Nature Phys.* **4,** 382–385 (2008).
25. Bishop, L. S. *et al.* Nonlinear response of the vacuum Rabi resonance. *Nature Phys.* **5,** 105–109 (2009).
26. Cohen-Tannoudji, C. & Reynaud, S. Dressed-atom description of resonance fluorescence and absorption spectra of a multi-level atom in an intense laser beam. *J. Phys. B* **10,** 345–363 (1977).
27. Zakrzewski, J., Lewenstein, M. & Mossberg, T. W. Theory of dressed-state lasers. I. Effective Hamiltonians and stability properties. *Phys. Rev. A* **44,** 7717–7731 (1991).
28. Mollow, B. R. Power spectrum of light scattered by two-level systems. *Phys. Rev.* **188,** 1969–1975 (1969).
29. Gonzalez-Tudela, A., Laussy, F. P., Tejedor, C., Hartmann, M. J. & del Valle, E. Two-photon spectra of quantum emitters. *New J. Phys.* **15,** 033036 (2013).
30. Gleyzes, S. *et al.* Quantum jumps of light recording the birth and death of a photon in a cavity. *Nature* **446,** 297–300 (2007).
31. Volz, T. *et al.* Ultrafast all-optical switching by single photons. *Nature Photon.* **6,** 605–609 (2012).
32. Majumdar, A., Englund, D., Bajcsy, M. & Vučković, J. Nonlinear temporal dynamics of a strongly coupled quantum-dot–cavity system. *Phys. Rev. A* **85,** 033802 (2012).
33. Del Valle, E., Gonzalez-Tudela, A., Cancellieri, E., Laussy, F. P. & Tejedor, C. Generation of a two-photon state from a quantum dot in a microcavity. *New J. Phys.* **13,** 113014 (2011).
34. Zubairy, M. S. & Yeh, J. J. Photon statistics in multiphoton absorption and emission processes. *Phys. Rev. A* **21,** 1624–1631 (1980).
35. Glauber, R. J. The quantum theory of optical coherence. *Phys. Rev.* **130,** 2529–2539 (1963).
36. Kavokin, A., Baumberg, J. J., Malpuech, G. & Laussy, F. P. *Microcavities* (Oxford Univ. Press, 2011).
37. Kubanek, A. *et al.* Two-photon gateway in one-atom cavity quantum electrodynamics. *Phys. Rev. Lett.* **101,** 203602 (2008).
38. Hong, H.-G., Nha, H., Lee, J.-H. & An, K. Rigorous criterion for characterizing correlated multiphoton emissions. *Opt. Express* **18,** 7092–7100 (2010).
39. Plenio, M. B. & Knight, P. L. The quantum-jump approach to dissipative dynamics in quantum optics. *Rev. Mod. Phys.* **70,** 101–144 (1998).
40. Wiersig, J. *et al.* Direct observation of correlations between individual photon emission events of a microcavity laser. *Nature* **460,** 245–249 (2009).
41. Srinivas, M. D. & Davies, E. B. Photon counting probabilities in quantum optics. *Opt. Acta* **28,** 981–996 (1981).
42. Zoller, P., Marte, M. & Walls, D. F. Quantum jumps in atomic systems. *Phys. Rev. A* **35,** 198–207 (1987).
43. Osad'ko, I. S. Photon distribution functions of fluorescence photons from single nanoparticles: three different photon counting methods. *Opt. Spectrosc.* **107,** 948–958 (2009).
44. Carmichael, H. *An Open Systems Approach to Quantum Optics* Ch. 6, 110 (Springer, 1993).
45. Loudon, R. *The Quantum Theory of Light* (Oxford Science Publications, 2000).
46. Ota, Y., Iwamoto, S., Kumagai, N. & Arakawa, Y. Spontaneous two-photon emission from a single quantum dot. *Phys. Rev. Lett.* **107,** 233602 (2011).
47. Laucht, A. *et al.* Electrical control of spontaneous emission and strong coupling for a single quantum dot. *New J. Phys.* **11,** 023034 (2009).
48. Nissen, F., Fink, J. M., Mlynek, J. A., Wallraff, A. & Keeling, J. Collective suppression of linewidths in circuit QED. *Phys. Rev. Lett.* **110,** 203602 (2013).
49. Del Valle, E. Distilling one, two and entangled pairs of photons from a quantum dot with cavity QED effects and spectral filtering. *New J. Phys.* **15,** 025019 (2013).
50. Boitier, F., Godard, A., Rosencher, E. & Fabre, C. Measuring photon bunching at ultrashort timescale by two-photon absorption in semiconductors. *Nature Phys.* **5,** 267–270 (2009).

Acknowledgements

The authors thank J. Sánchez Wolff for assistance with Fig. 1. This work was supported by the POLAFLOW European Research Council starting grant, the Marie-Curie project Sensing Quantum Information Correlations and the Spanish Ministerio de Economía y Competitividad (MAT2011-22997). C.S.M. acknowledges a Formación de Personal Investigador grant. A.G.T and K.M. acknowledge support from the Alexander Von Humboldt Foundation and F.P.L. acknowledges support from a Ramón y Cajal contract.

Author contributions

F.P.L. and E.d.V. proposed the idea. C.S.M., E.d.V. and F.P.L. developed the theoretical formalism and the conceptual tools. C.S.M. implemented the theoretical methods and analysed the data. A.G.T., K.M., S.L., M.K. and J.J.F. contributed material, analysis tools and expertise. F.P.L., C.S.M., E.d.V., C.T. and J.J.F. wrote the main paper. C.S.M., E.d.V., A.G.T. and F.P.L. wrote the Supplementary Information. F.P.L. supervised the research. All authors discussed the results and its implications and commented on the manuscript.

Additional information

Supplementary information is available in the online version of the paper. Reprints and permissions information is available online at www.nature.com/reprints. Correspondence and requests for materials should be addressed to F.P.L.

Competing financial interests

The authors declare no competing financial interests.

nature photonics

SUPPLEMENTARY INFORMATION

DOI: 10.1038/NPHOTON.2014.114

Emitters of N-photon bundles
Supplementary Information

C. Sánchez Muñoz,[1] E. del Valle,[1] A. González Tudela,[2] K. Müller,[3]
S. Lichtmannecker,[3] M. Kaniber,[3] C. Tejedor,[1] J.J. Finley,[3] and F.P. Laussy[1]

[1] *Condensed Matter Physics Center (IFIMAC), Departamento de Física Teórica de la Materia Condensada, Universidad Autónoma de Madrid, 28049 Madrid, Spain*
[2] *Max-Planck-Institut für Quantenoptik, Hans-Kopfermann-Str. 1, 85748 Garching, Germany*
[3] *Walter Schottky Institut, Technische Universität München, Am Coulombwall 4, 85748 Garching, Germany*

I. GIANT RABI OSCILLATIONS BETWEEN ARBITRARILY DISTANT MANIFOLDS.

Without dissipation, the coherent driving at low intensity of the detuned cQED system probes the Jaynes–Cummings resonances. This leads to giant Rabi oscillations between the vacuum state $|0\mathrm{g}\rangle$ on the one hand and the quantum emitter (QE)'s excited state with N photons in the cavity $|N\mathrm{e}\rangle$, on the other hand. Since N can be any integer, depending on which resonance is driven, the superposition is between states that differ arbitrarily in energy:

$$|\psi_N\rangle = \frac{1}{\sqrt{2}}\left(|0\mathrm{g}\rangle + |N\mathrm{e}\rangle\right) . \qquad (1)$$

Such a superposition has been hypothetically referred to describe "spooky" features of quantum mechanics, like non-conservation of energy (the collapse of such a wavefunction suddenly realizes a state that has either no energy or the huge amount $\hbar\omega_\sigma + N\hbar\omega_a$) [1, 2]. We provide here a mechanism to actually realize it.

The ease in setting up the state Eq. (1), that would require extremely difficult operations with little chances of success with a direct engineering [3], is to be atoned by the timescales involved. The Rabi oscillations become vanishingly slow for increasing differences of energy. In what follows, we derive analytical expressions for their frequencies.

In the rotating frame of the laser, the Hamiltonian becomes $H = \delta_a a^\dagger a + \delta_\sigma \sigma^\dagger\sigma + g(a^\dagger\sigma + \sigma^\dagger a) + \Omega(\sigma^\dagger + \sigma)$ and we are left with solving Schrödinger equation $|\dot{\psi}\rangle = -iH|\psi\rangle$, whose formal solution in the basis of the eigenstates $|\phi_i\rangle$ of H reads:

$$|\psi(t)\rangle = c_1|\phi_1\rangle e^{-iE_1 t} + c_2|\phi_2\rangle e^{-iE_2 t} + \cdots \qquad (2)$$

with the coefficients $c_i = \langle\phi_i|\psi_0\rangle$ to be determined by the initial state $|\psi_0\rangle$. Using the basis of bare states, $\{|0\rangle, |1\rangle, |2\rangle, |3\rangle, \ldots\} \equiv \{|0\mathrm{g}\rangle, |0\mathrm{e}\rangle, |1\mathrm{g}\rangle, |1\mathrm{e}\rangle, \ldots\}$, one can represent the wavefunction through the probabilities p_i for the system to be in the state $|i\rangle$:

$$p_i(t) = |\langle i|\psi(t)\rangle|^2 = \sum_{j,k} c_j c_k^* \langle i|\phi_j\rangle\langle\phi_k|i\rangle e^{i(E_k - E_j)t} . \qquad (3)$$

While in general, to first approximation, the system remains trivially in the ground state, one finds that for certain frequencies of excitation, ω_N, there is a striking change to full-magnitude Rabi oscillations, with $p_{0g} = p_{Ne} = 1/2$ and all other $p_k = 0$. This is the case whenever the laser hits a $(N+1)$-photon resonance of the Jaynes–Cummings ladder, as explained in the main text. In the purely Hamiltonian picture, such resonances can be revealed by plotting the amplitude of the Rabi oscillations, that is, their time average which is given by the sum of the non-oscillating terms in Eq. (3), i.e., $\langle p_i\rangle = \sum_j |c_j|^2 |\langle i|\phi_j\rangle|^2$. These are displayed in Fig. S1 and are in direct correspondence with the resonances in $g^{(n)}$ shown in Fig. 3c of the text. This implies that this giant Rabi dynamics of distant manifolds is responsible for the strong N-photon correlations in the detected field when opening the dissipative channel. One can see neatly how the laser "strikes different quantum chords" and brings in resonance the vacuum (upper red curve) with each one of the manifolds in succession, climbing the Jaynes–Cumming ladder in the process. There is a neat transition from the quantized nature of the cavity QED system on the QE side, on the right of the Fig. S1a, towards a continuum as it bridges to the classical field of the cavity, on the left. Note that the resonances widths decay exponentially with the number of photons in the superposition and

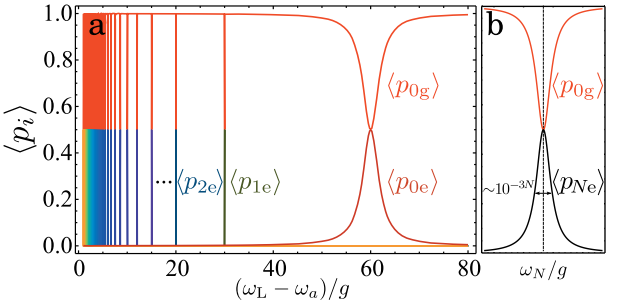

FIG. S1: **a**, Probability of occupation of the states $\{|0\mathrm{g}\rangle, |0\mathrm{e}\rangle, |1\mathrm{g}\rangle, \ldots\}$ as a function of the excitation frequency. This shows how the laser can "strike" quantum resonances to trigger full-amplitude Rabi oscillations between the vacuum $|0\mathrm{g}\rangle$, in red, and any of the excited states $|N\mathrm{e}\rangle$. The multi-photon resonances of states with N photons in the cavity have a width of the order of 10^{-3N}. They thus appear as straight vertical lines on the scale of panel a. A magnification of a generic resonance is shown in **b**.

DOI: 10.1038/NPHOTON.2014.114

are thus extremely sharp, appearing like δ functions in the plot. A magnification of a generic resonance is provided in Fig. S1b.

Such strong resonances suggest a change in the structure of the energy levels induced by the laser, which result, at certain frequencies, in the isolation of the two states involved in the N-polariton state (1). A convenient way to study analytically such an emerging manifold structure is to resort to the Hamiltonian H in the rotating frame of the laser in the limit $\Omega \to 0$. The information of how the states are coupled when the laser is switched on is encoded in the eigenenergies $E^n_\pm - n\omega_{\rm L}$ now explicitely dependent on the laser frequency. All the resonances occur when two eigenenergies cross, yielding the resonant frequencies:

$$\omega^{n,\xi}_{n',\xi'} = \omega_a + \frac{\xi\sqrt{ng^2+\Delta^2/4} - \xi'\sqrt{n'g^2+\Delta^2/4}}{n-n'}\,, \quad (4)$$

with n, $n' \in \mathbf{N}$ (and $n \neq n'$) and ξ, $\xi' \in \{-1, 1\}$ corresponding to lower and upper polaritons, respectively. The ground state is given by $\xi = -1$, $n = 0$. This predicts more resonances than those plotted in Fig. S1, that appear as satellite peaks to the main resonances which are $\omega_N = \omega^{N+1,1}_{0,-1}$. The additional resonances are indeed observed when zooming in on the appropriate range. They are small as they do not realize full-amplitude Rabi oscillations, and correspond to n-photon transitions between two manifolds not involving the ground state. These peaks would yield full Rabi oscillations if the initial state would be chosen adequately.

Since an isolated manifold emerges at each resonance, whose dynamics can be well separated from the rest of the states, we can perform an adiabatic elimination to retain only the coupling between the relevant states and derive an effective Hamiltonian that provides the Rabi frequencies. We will treat the case of $|\psi_2\rangle$ explicitly. In that situation, it is enough to restrict ourselves up to the second manifold, and use for the solution the ansatz $|\psi(t)\rangle = \sum_{i=0}^{4} c_i(t)|i\rangle$. The Schrödinger equation for the coefficients reads:

$$i\begin{pmatrix}\dot{c_1}\\ \dot{c_2}\\ \dot{c_3}\\ \dot{c_4}\\ \dot{c_5}\end{pmatrix} = \begin{pmatrix}0 & \Omega & 0 & 0 & 0\\ \Omega & \delta\sigma & g & 0 & 0\\ 0 & g & \delta_a & \Omega & 0\\ 0 & 0 & \Omega & \delta_\sigma+\delta_a & \sqrt{2}g\\ 0 & 0 & 0 & \sqrt{2}g & 2\delta_a\end{pmatrix}\begin{pmatrix}c_1\\ c_2\\ c_3\\ c_4\\ c_5\end{pmatrix}.$$

Setting $\dot{c_1} = \dot{c_2} = \dot{c_4} = 0$, one can eliminate c_1, c_2 and c_4 from the system of differential equations, and get the corresponding effective Hamiltonian:

$$H_{\rm eff} = \begin{pmatrix} \frac{\Omega^2}{\delta_\sigma(1-g^2/(\delta_a\delta_\sigma))} & \frac{g\Omega^2}{\delta_a\delta_\sigma}\left(\frac{1}{1-g^2/(\delta_a\delta_\sigma)}\right) \\ \frac{g\Omega^2}{\delta_a\delta_\sigma}\left(\frac{1}{1-g^2/(\delta_a\delta_\sigma)}\right) & \delta_a+\delta_\sigma-\frac{g^2}{\delta_a}+\left(\frac{1}{1-g^2/(\delta_a\delta_\sigma)}\right)\frac{\Omega^2}{\delta_a}\end{pmatrix}. \quad (5)$$

The Rabi frequency for the two photon resonance is thus obtained as:

$$\Omega^{(2)}_{\rm eff} = \frac{g\Omega^2}{\delta_a\delta_\sigma - g^2}\,. \quad (6)$$

If $\delta_a, \delta_\sigma \gg g, \Omega$, the Rabi frequency takes the form $(\sqrt{g}\Omega)^2/(\delta_a\delta_\sigma)$ of a generalized Lamb shift for the Jaynes–Cummings model, that is, it shows the energy shift of the coupled light-matter system by the driving laser as opposed to the conventional scenario where the light mode shifts the QE alone.

Following the same procedure for the next manifolds of excitation, the Rabi frequency up to any order can be obtained analytically as:

$$\Omega^{(n)}_{\rm eff} = \frac{g^{n-1}\Omega^n\sqrt{(n-1)!}}{D_{2(n-1)}}\,, \quad (7)$$

where D_n is defined through the recurrence relation $D_n = a_nD_{n-1} - b_n^2D_{n-2}$ with $D_0 = 1$, $D_1 = a_1$ with:

$$a_n = \begin{cases}\delta_\sigma + \frac{n-1}{2}\delta_a\,,\\ \frac{n}{2}\delta_a\,,\end{cases} \quad b_n = \begin{cases}-\Omega\,, & n \text{ odd}\\ \sqrt{\frac{n}{2}}g\,, & n \text{ even}\end{cases}$$

resulting in exact expressions easily obtained but too heavy to write here. Approximated versions in the limit of large detunings are much simpler, such as the Rabi frequency for $|\psi_3\rangle$:

$$\Omega^{(3)}_{\rm eff} \approx \frac{g^2\Omega^3}{\sqrt{2}(\delta_a^3\delta_\sigma + \delta_a^2\delta_\sigma^2)}\,. \quad (8)$$

This completes the characterization of the remarkable states of Eq. (1). The quantum superposition between the vacuum and a highly excited state is possible, although it involves very sharp resonances with slow Rabi oscillations. We proceed to the case where such resonances can be brought to immediate use for actual devices, thanks to dissipation.

II. TRANSITION FROM THE JAYNES–CUMMINGS DYNAMICS TO THE MOLLOW DYNAMICS.

The Hamiltonian used in this work covers fully and bridges between two pillars of quantum nonlinear optics, namely, the Jaynes–Cummings model on the one hand and the Mollow physics of the dressed atom on

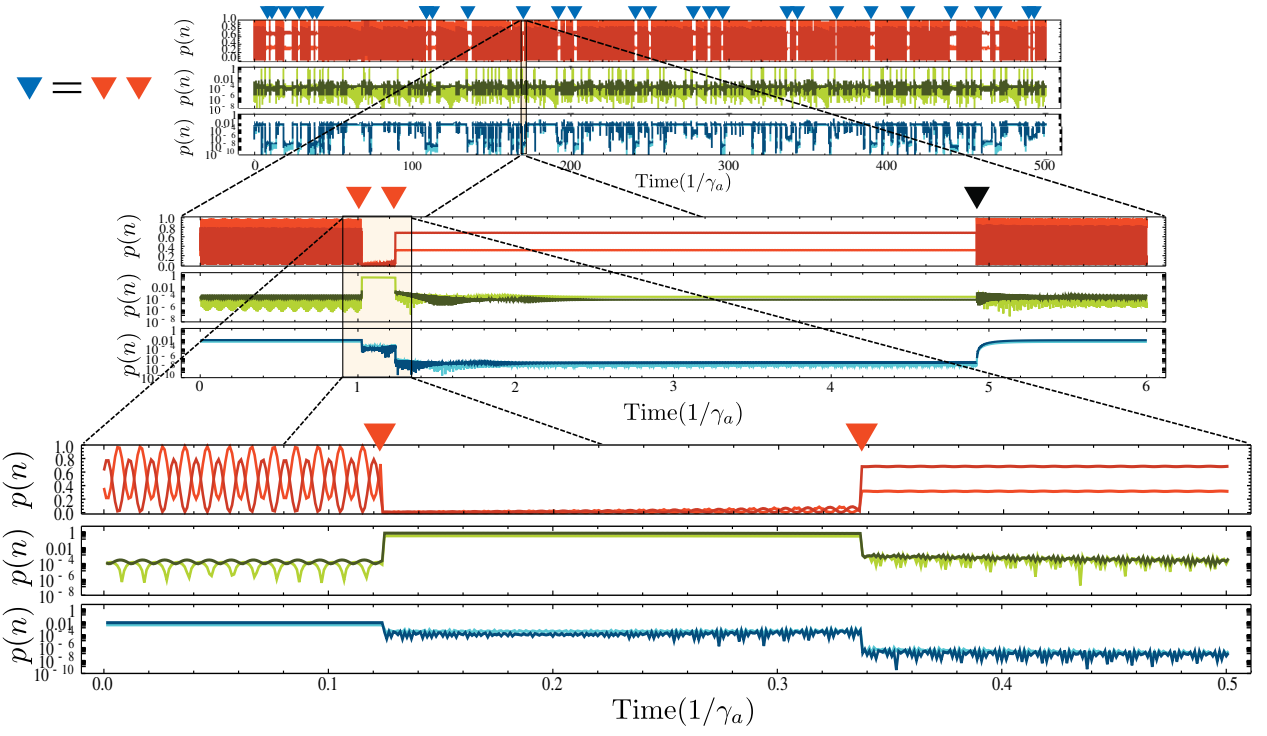

FIG. S2: (Colour online) Quantum trajectory showing the different timescales involved in the mechanism of two-photon emission. The colour code and notations are the same as Fig. 4a–c of the text. Top: long time-range dynamics. Two-photon events are identified as blue triangles while the underlying single-photons are identified as red triangles. Emission from the QE is shown as a black triangle. Statistics of these events are given by the two-photon second order correlation function $g_2^{(2)}(\tau)$. Medium: White stripes are due to the absence of Rabi flopping of the QE after the second cavity emission, and its length is given by the QE lifetime. After a subsequent QE emission, the Rabi flopping is restored and the construction of a new two-photon state in the cavity is resumed. This manifests as a dependence of the statistics of the two-photon bundles on the QE lifetime (Fig. S6a). Bottom: The shortest timescale on the dynamics is given by the Mollow frequency, that precedes the sequence of rapid two photons emission.

the other hand. The transition is rich and complicated and this work certainly does not exaust it. It is maybe better comprehended by following the resonances themselves, as the laser intensity is tuned up. This is shown in Fig. 3a of the text for three pumping values and is provided for all pumpings in the movie `JCMollowTransition.mp4`. The system starts at low pumping intensity with resonances at ω_N [cf. Eq. (1) from the text]. Each resonance corresponds to a giant Rabi oscillations described by Eq. (1). In this regime, the resonances in $g^{(n)}$ at various $\omega_{\rm L}$ (shown in the animation for $n = 2$) change magnitude relatively to each other with increasing pumping but stay pinned to the Jaynes–Cumming ladder. At some point, the laser takes over the cavity, resulting in a blueshift of the resonances due to state dressing. This is the transition to the Mollow regime. At large pumping, the cavity that was previously constituting half of the system along with the QE, becomes a mere Purcell enhancer of the dynamics, now dominated by the laser that is driving the QE. Note that the QE always remains the central actor: the quantum character of the emission comes from the QE, while the cavity, or the laser, are classical probes or catalysts, that trigger, store and convey the engineered emission from the active material [4].

The transition is also pictured from an alternative point of view in Fig. 4a–c, through the probabilities derived from the wavefunction. The Jaynes–Cummings limit, Fig. 4a, is simply the superposition of two states. The Mollow limit, Fig. 4b, exhibits a more complicated dynamics that involves a fast Rabi flopping of the dot and starts to mix more states from various manifolds, but still keeping the feature of involving only a few of them. The same limit with dissipation, Fig. 4c, is the case that realizes N-photon emission. The excitation of the multi-photon resonances in this case brings in succession various regimes that evolve with different timescales, and between which the system transits by collapse of the wavefunction. This is shown in Fig. S2, that displays a long portion of one quantum trajectory (top) that is expanded successively for regions of interest (from top to bottom). The top panel depicts the bundle emission, indicated by blue triangles, at the timescale of detection. This appears as white stripes in an otherwise fast oscillating dynamics. Zooming in on such a stripe, second row, one see that the bundle

DOI: 10.1038/NPHOTON.2014.114

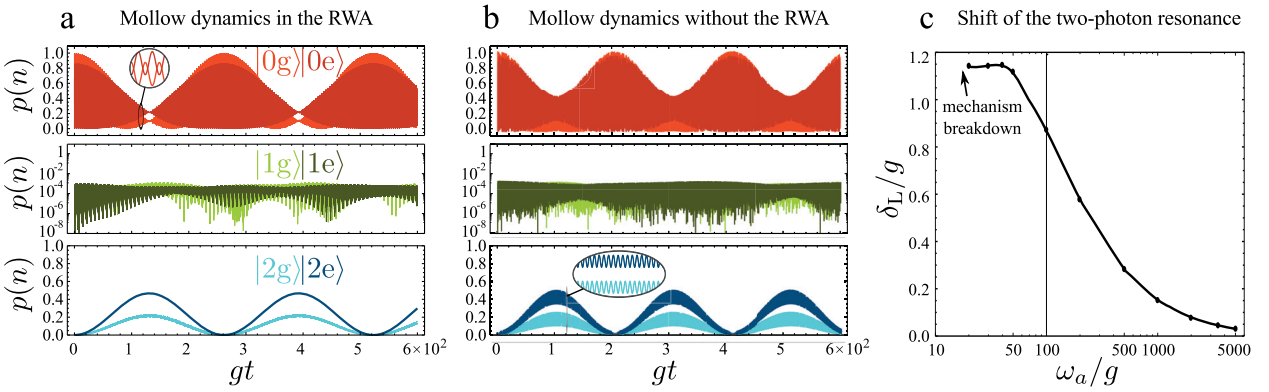

FIG. S3: **a**, Dynamics of the strongly-driven and largely detuned system within the RWA (panel b of Fig. 4 in the main text). **b**, The corresponding dynamics without the RWA in the USC regime for $\omega_a/g = 100$. While the counter-rotating terms have an observable difference (starting with ratio $\omega_a/g \lesssim 2000$), the phenomenology remains essentially the same. **c**, Shift δ_L of the laser frequency ω_L to trigger the two-photon resonance, caused by the counter-rotating terms in the Mollow regime of strong driving. At about $\omega_a/g \approx 20$, the mechanism breaks down and fails to produce a two-photon resonance with large amplitude Rabi oscillations. This is the regime where the RWA fails completely.

is composed of two single-photons, depicted as red triangles. This window contains the two-photon emission iself, on a short timescale, followed by the reloading time, ruled by the QE. This determines the statistics of bundle emission. Finally, zooming in on the two-photon emission itself, last row, one can resolve the characteristic time of the two-photon emission process, given by the cavity lifetime. The shortest timescale is that of the Mollow Rabi floping, which governs the dynamics most of the time, and whose jolting by the quantum collapse provokes an avalanche of two-photon emission.

III. VALIDITY OF THE ROTATING WAVE APPROXIMATION.

The Jaynes–Cummings description is a simplified model which, despite its various approximations, has proved extremely successful in describing a large body of experiments which belong to the paradigm of a two-level system interacting with an harmonic mode [5]. The model can be subsequently extended and upgraded with features to account for more realistic situations, such as multiple-modes or many-body correlations [6–8] (see also Section VI that includes in this way effects of noise and decoherence), but the core of our effect can be tracked down to the Jaynes–Cummings physics itself.

One of the fundamental approximations that is performed at a very early stage of the model is the so-called Rotating Wave Approximation (RWA) [9], that neglects the counter-rotating terms of the light-matter interaction of the type $a\sigma$ and $a^\dagger\sigma^\dagger$, rapidly oscillating, as compared to the terms $a\sigma^\dagger$ and $a^\dagger\sigma$, which balance the frequencies of the modes at resonance. The approximation can lead to deviation from the actual result when the system is extremely far from resonance and/or when the frequency of the free oscillators is comparable to the exchange rate of excitation (coupling strength), in which case the system enters the regime of Ultra Strong Coupling (USC) [10, 11]. The RWA may also be an issue in the dynamics of the strongly driven two-level system alone, where deviations from the approximation manifest as the Bloch-Siegert shift [12]. Since our system invokes both strong driving of the QE on the one hand and detuning on the other hand, we must consider the validity and effect of the RWA.

The validity of the RWA for the strongly driven Jaynes–Cummings model has been studied in the literature [13, 14]. The counter-rotating terms were found to be important in the USC regime, for ratios of ω_a/g of order at least 10. For the three platforms of choice that we consider for our effect, one deals with ratios of typically several hundreds for superconducting qubits in a microwave resonator [15, 16], tens of thousands and above for quantum dots in microcavities [17] and millions and above for atoms [18]. For quantum dots and atoms, we are extremely far from the USC and the counter-rotating terms can be safely ignored. Superconducting qubits are closer to the regime where these term could matter, being indeed systems of choice to approach the USC regime with the possibility to get to the regime where the RWA breaks down completely [10]. To investigate the relevance of our system also for these systems sensitive to the RWA, we have performed numerical calculations that simultaneously take into account the counter-rotating terms for both the detuned QE-cavity coupling on the one hand and the driven QE on the other hand. We show in Fig. S3 the regime where the approximation is the less accurate, that is, at high driving intensity for a superconducting qubit situation where $\omega_g/g = 100$ (the deviation starts to be unnoticeable for values of

$\omega_a/g \gtrsim 2000$). The dynamics with RWA, which is the case of the text, is compared to that without the approximation. While the counter-rotating terms do affect the result, the effect is surprisingly resilient and retains its qualitative features. Indeed, the non-RWA dynamics mainly consists in a superimposition of very fast oscillations on top of the RWA dynamics, leading to a mere broadening of the oscillations. There is also a small renormalization of the frequencies, that is due to the shift of the resonance itself, shown in Fig. S3c. It takes counter-rotating terms of the order of a fraction of the detuning itself to completely spoil the effect and reach a dynamics that differs in essential terms from that of the RWA. This suggests that our scheme could be usefully transported till far into the USC regime where it could set the arena for interesting physics. Note that the problem of a proper theoretical model to describe the dissipative regime of an USC cavity QED setup is still open to debate [11, 19, 20] and the theoretical analysis of the output of such a device is thus way beyond the scope of this Supplementary Information.

IV. THE RELATION OF THE "BUNDLE" TO A FOCK STATE.

There are differences between the concept of a N-photon Fock state $|N\rangle$ and a bundle, as discussed in the main text. A Fock state $|N\rangle$ is a well defined object that does not account for any internal degree of freedom, while the bundle is the result of a dynamical process and henceforth it has an intrinsic temporal structure. This stems from the radiative cascade that gives rise to the emission of a bundle, which is clearly manifested as blocks emerging in the diagonal of the density matrix (see Fig. 5b). When the intracavity dynamics is dominated by this cascade events (as is the case in the regime of pure N-photon emission), the steady state probability of finding n photons inside the cavity is given by $p(n) = n_a/(Nn)$, cf. Eq. (5) in the text. In good approximation, $p(0) = 1 - \sum_{i=1}^{N} p(n)$ since probabilities for higher n are much smaller than those of the vacuum and the cascade of the bundle emission. Note that n_a/N is the bundle population. This probability is the result of a time-averaging over all cycles of the dynamics and is thus the one encoded in the diagonal element of the cavity density matrix, which is easily obtained from the master equation. The equation predicts a line in the graph of $p(n)$ when plotted as a function of $1/n$, as shown in Fig. S4a, rather than the peaked Kronecker distribution for a Fock state. The slope of the line corresponds to the bundle population n_a/N and its length to the number of photons in the bundle. Deviations from a straight line indicate a purity lower than 100%.

As mentioned in the main text, these internal correlations have a signature in the different time intervals that separate the photons if they are individually detected. The time separation between the photons composing a bundle is sketched in Fig. 5c in the main text. This structure can be seen from the collected Monte-Carlo events by plotting the probability distribution of the detection of two successive photons with a given time difference, as is done in Fig. S4b, that shows a N-exponential decay for the cases of $2 \leq N \leq 4$-photon emission. One observes that the jitter imposes its largest toll for the case $N = 2$, since a bundler of N-photon is wrapped up in a time window of H_N/γ_a only (H_N is the Nth harmonic number, e.g., the overall lifetime is $\approx 2.28/\gamma_a$ for a bundle of five photons and is still smaller than $3/\gamma_a$ for a fat bundle of ten photons).

One can characterize alternatively the quantum state of the cavity field alone by turning to the Wigner distribution, which provides a self-contained and insightful

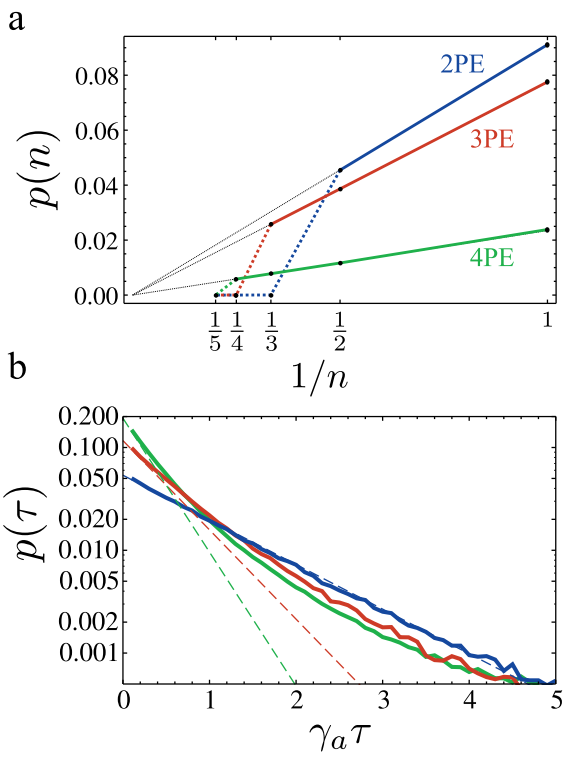

FIG. S4: (Colour online) Signatures of the internal structure of the N-photon bundles **a**, Diagonal elements of the cavity density matrix $p(n) = \langle n|\rho|n\rangle$ in the regimes from two to four-photon emission. Plotted as function of $1/n$, and according to Eq. (5) of the text, this yields a line in the regime of 100% purity with a slope equal to the bundle population n_a/N and extent equal to the number N of photons per bundle. **b**, Distribution of time intervals τ between successive photons of a bundler, in the regimes of two (blue), three (red) and four (green) photon emission. The distributions are $(N-1)$-exponential for N-photon emission, i.e., exponential for $N = 2$, bi-exponential for $N = 3$, etc. This confirms the time-distribution of the photons within the bundles as sketched in Fig. 5c in the main text. Thin lines show the $\exp(-(N-1)\tau)$ decay, to which the distributions get parallel to. The distribution of four-photon emission (green), for instance, gets parallel to all three lines in successive intervals.

DOI: 10.1038/NPHOTON.2014.114

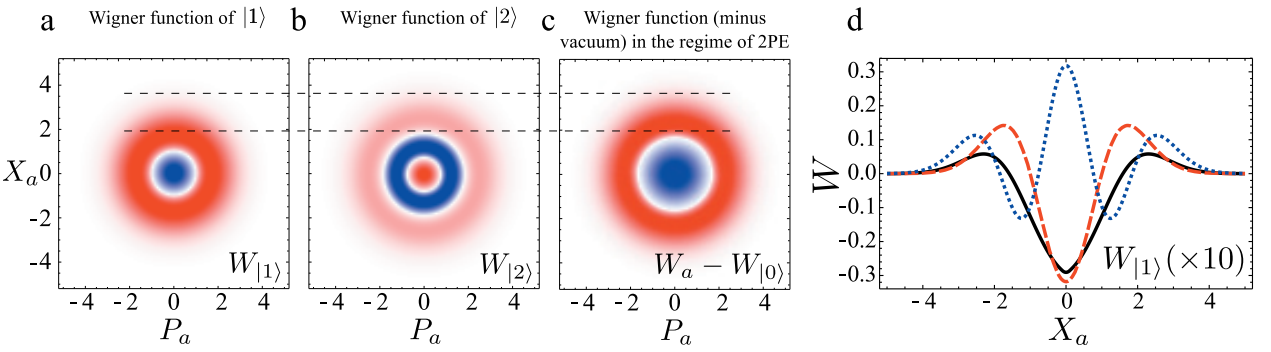

FIG. S5: (Colour online) Quantum state of the N–photon emitter. **a**–**c**, Wigner representation of the cavity field, comparing the Wigner distribution of the Fock states $|1\rangle$ (a) and $|2\rangle$ (b) with that of the cavity field in the regime of two-photon emission, to which we removed the predominant Wigner function of the vacuum. As also seen in the cut along a radius in **d**, the Wigner function of the two-photon emitter (solid black) is qualitatively similar to the Fock state $|1\rangle$ (dashed red) but with some attributes of Fock state $|2\rangle$ (dotted blue).

phase-space representation in the complex plane $\alpha = (X + iP)/2$ with X and P the quadratures [21]. The Wigner representation for the Fock projector $|m\rangle\langle n|$ is:

$$W_{mn}(r,\phi) = \frac{(-1)^n}{\pi}\sqrt{\frac{n!}{m!}}e^{i\phi(m-n)}r^{m-n}L_n^{m-n}r^2e^{-\frac{r^2}{2}}, \tag{9}$$

with $m \geq n$ ($W_{nm} = W^*_{mn}$) and $L_n^{m-n}(r^2)$ Laguerre polynomials. The Wigner function for the reduced density matrix $\rho = \sum_{mn}\rho_{mn}|m\rangle\langle n|$ is then $W = \sum_{mn}\rho_{mn}W_{mn}$. From this expression, one sees that the Wigner function of the Fock state $|N\rangle$ is described essentially by the Laguerre polynomials $\frac{(-1)^n}{\pi}L_n^0(r^2)e^{-r^2/2}$. Since $L_n^0(r^2)$ has $2n$ roots, the largest one of which being $\propto \sqrt{n}$, the associated Wigner function features $2n$-nodes contained in an annulus of mean radius $\sqrt{n}$, cf. Fig. S5a–b. The Wigner representation of the cavity field in our case features again predominantly the vacuum, given the underlying mechanism. By removing this vacuum so as to magnify the small structure due to the N-photon emission, one sees that the result resembles a Fock state $|1\rangle$, with the same number of nodes as its Wigner function, but with a size comparable to that of the Fock state $|2\rangle$, as shown in Fig. S5(a–c). We have checked that the same pattern holds for higher regimes of N-photon emission, namely, one-node circularly symmetric Wigner function with a radius that grows like the square root of N. This indicates the peculiar character of the state that gives rise to the bundle emission, mixing both attributes of, and departure from, the Fock state itself. The symmetric Wigner distribution is achieved in the regime of N-photon emission, with features mainly given by the diagonal elements of the cavity density matrix, Eq. (5) in the main text. It is surrounded by states with an intricate structure when not in the regime of 100% purity, as seen in the supplementary video `BundleQuantumState.mp4`.

Now that we have shown that our emitter produces states which are not strictly Fock states, we must balance the discussion by showing that there remains a deep connection with this concept. It is maybe best illustrated with the form of the generalized correlation function $g_N^{(n)}$, Eq. (6) of the text. While the term a^N appears nowhere explicitly in the Hamiltonian or any other part of the dynamics, it enters the correlation function that describes the statistics of emission and a in isolation plays no role by itself. Now, $(a^N)^\dagger$ is precisely the operator that creates a Fock state from the vacuum:

$$|N\rangle = \frac{(a^N)^\dagger}{\sqrt{N!}}|0\rangle\,. \tag{10}$$

The statistics of the bundles is therefore described by a quantity where the photon operator itself does not enter but needs to be upgraded to a Fock state creation operator. This demonstrates that there is a strong connection between a bundle and a Fock state of N photons. Surprisingly, while we could expect that a correlation function built on a^N operators would break for correlation times smaller than the coherence time of the bundle, that is, for $\tau \ll 1/\gamma_a$, the agreement remains perfect down to $\tau = 0$ coincidences. This suggests that regardless of the internal structure of the bundle, it is perceived as a Fock state in a measurement integrated over a small time window, or simply because of the time uncertainty in the detection. This is in agreement with the production of Fock states from mechanisms such as the joint emission of N atoms from an excited state [22]. One could establish this fact on firmer theoretical grounds by studying the indistinguishability of two bundles emitted by the system or of a bundle with an exact Fock state, by computing HOM interferences between the two arms of a beam-splitter. Such analyses have been conducted only recently in a dynamical setting [23] and their extension to characterize the output of an emitter, such as our N–photon source, will be presented in a future publication.

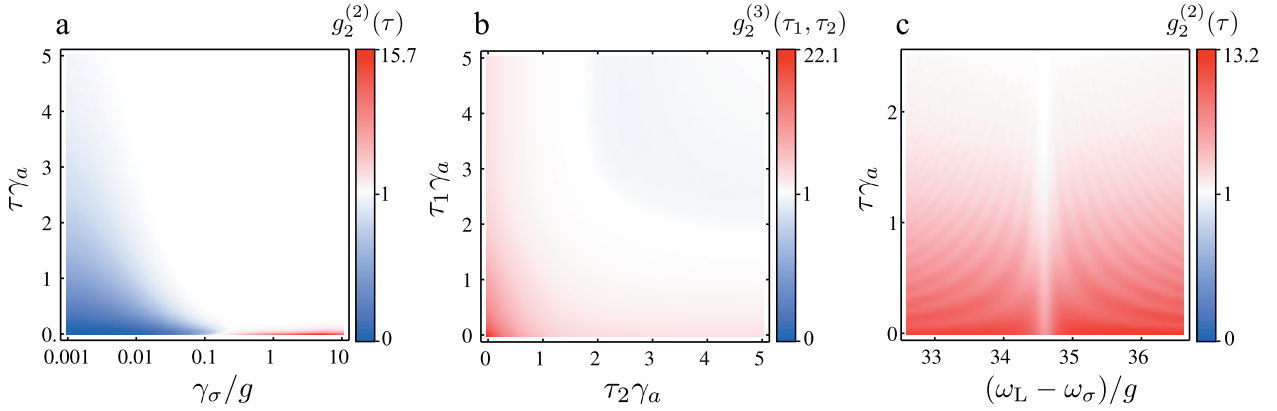

FIG. S6: **a**, Second order bundle correlation function $g_2^{(2)}(\tau)$ as a function of the QE decay rate γ_σ, showing how the emitter covers various regimes from antibunching of two-photon emission for lower γ_σ to bunching of two-photon emission for larger γ_σ, passing by coherent emission, $g_2^{(2)}(\tau)=1$ at intermediate $\gamma_\sigma \approx 0.2g$. Figures 3(h–i) in the text correspond to two vertical cuts at $\gamma_\sigma/g=0.01$ and $\gamma_\sigma/g=0.2$ of this figure. **b**, Third order bundle correlation function $g_2^{(3)}(\tau_1,\tau_2)$ at $\gamma_\sigma/g=0.2$. The correlation is unity except in a small window at small τ's due to the cavity jiter, supporting that the bundle emission is coherent to all orders. **c**, Bundle emission is coherent only when hitting the resonance, at $\omega_L \approx \omega_a + 34.6g$, and displays a given, but no particular in any sense, dynamics out of resonance.

Finally, we have addressed before the question of the quantum state of one bundle. One could also pose the problem of the quantum state of the stream of the emission, which is however even more involved as it requires to describe the quantum state of the output field itself and therefore a non-trivial extension of the model. One can think, for instance, to study the quantum state of a quantum oscillator initially at rest, after its excitation for a given time by the emitter in the regime of N-photon emission. It is expected to produce a coherent superposition of multiples of N photons, that is to say, a brand of squeezing. All these questions are relevant for quantum applications and remain to be fully explored.

V. HIGHER ORDER N-PHOTON CORRELATIONS.

In the main text, we have established that the proposed emitter substitutes the basic unit of excitation of the light field—the photon—by the bundle (a packet of N photons), and that the conventional tools of quantum optics have to be upgraded consequently. Namely, the standard photon statistics when the system is in a regime of N-photon emission provides no particular result, while the bundle-statistics behaves in a meaningful way. We have stated that the bundle statistics can be tuned with the QE lifetime $1/\gamma_\sigma$. This is substantiated with Fig. S6a, that shows how $g_2^{(2)}(\tau)$ evolves from antibunched when γ_σ is small to bunched when it is large, passing by the regime of coherent emission in between, with $g_2^{(2)}(\tau)=1$. In the later case, the bundles are randomly distributed, which means that the emitter is coherent, in the sense of Glauber who understood that quantum optical coherence is linked to the statistics of the quanta, rather than to monochromaticity. This criterion is now commonly accepted to define lasing, for instance, the "atom laser" refers to a coherent matter wave, not to stimulated emission. To rigorously qualify our source as a laser of N-photon states, we have to show that the bundles are Poisson distributed not only at the level of pairs of bundles, i.e., that $g_2^{(2)}(\tau)=1$ as was shown in the text, but to all orders. This is shown in Fig. S6b with $g_2^{(3)}(\tau_1,\tau_2)$ that is seen to be close to 1, except in the jitter window (at small τ's), where the bundle can be resolved into its underlying photons. Since $g^{(n)}$ magnifies correlations as n increases, the approximation to a white square (corresponding to an ideal coherent signal) is actually excellent. Outside of the resonance, when the system does not behave as a N-photon emitter, the generalized correlation functions $g_N^{(n)}$ show no particular feature. This is illustrated in Fig. S6c for the case of lasing, where the sharp vertical line at $(\omega_L-\omega_a)/g \approx 34.6$ shows coherent bundle emission when hitting the resonance. The second order correlation function of the cavity field is not equal to one in the regime of coherent bundle emission (Fig. 4h of the text), so the cavity emission is not coherent if counting photons one by one. It becomes so at the N-photon level.

VI. EFFECT OF DECOHERENCE.

We have presented the scheme so far in an ideal system that suffers from no source of noise or decoherence apart from decay. It is one of the challenges of technology to keep these under control or remove them altogether to achieve any working quantum technology. It is still useful, however, to judge the present day feasi-

DOI: 10.1038/NPHOTON.2014.114

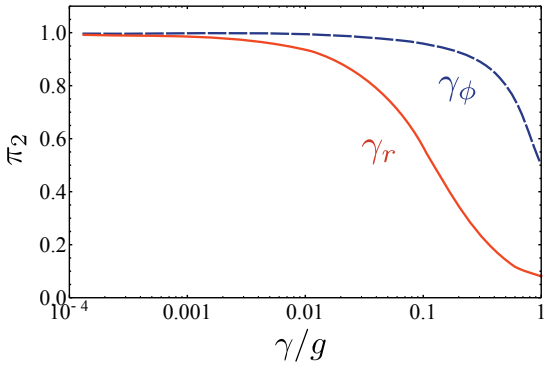

FIG. S7: (Colour online) Effect of the principal sources of noise in a semiconductor platform on the purity of two-photon emission in the regime where it is optimum. Rates of pure dephasing γ_ϕ (dashed blue) and cavity feeding at positive detuning γ_r (solid red) are varied independently up to the Rabi rate g of resonant exchange between the dot and the cavity. The mechanism is very robust against the generic source of decoherence that is pure dephasing γ_ϕ and is more sensible to cavity feeding γ_r. Values from the literature show that one can expect extremely performing N–photon emitters already with currently available samples.

bility of the proposed device by considering the impact of noise on its efficiency. We study in this Section the effect of both a generic source of decoherence, pure dephasing [8, 24], and of a particular source that is specific to semiconductor cavity QED in the configuration of our study, namely, cavity feeding [7, 25–28]. The former washes out the quantum coherence that links pure states, leading to a mixed density matrix. It is caused by a variety of detrimental agents, such as weak coupling to external baths, interactions, etc., and could be present to some extent in all experiments regardless of their implementation. The latter, cavity feeding, is proper to semiconductors and can be important even with a large detuning between the QE and the cavity. It is caused by the phonon-mediated transfer of an excitation between the QE—in this case, a quantum dot—and the cavity. The transfer can be predominant either from the QE to the cavity or the other way around depending on the detuning. The configuration of negative detuning Δ, when the dot is blue-detuned as compared to the cavity, is particularly harmful to the mechanism, since this is the one that transfers mainly towards the cavity due to an unavoidable spontaneous emission, therefore spoiling it with uncorrelated events. The reversed process, that transfers towards the dot, is assisted by the population of phonons available at the transition frequency $n_{\rm ph}(\Delta) = 1/(e^{\Delta/[k_{\rm B}T]} - 1)$ with no spontaneous emission term, and can thus be made small by lowering the temperature T. On the other hand, with negative detuning, the importance of these processes is reversed. As the scheme presented in the text is otherwise symmetric with respect to detuning, we will consider only the favourable red-detuned configuration. The model is extended to include these sources of decoherence and dephasing by adding to the master equation the three terms of the second line [7]:

$$\dot\rho = -i\,[H,\rho] + \Big[\frac{\gamma_a}{2}\mathcal{L}_a + \frac{\gamma_\sigma}{2}\mathcal{L}_\sigma + \frac{\gamma_\phi}{2}\mathcal{L}_{\sigma^\dagger\sigma} + \frac{(1+n_{\rm ph})\gamma_r}{2}\mathcal{L}_{\sigma^\dagger a} + \frac{n_{\rm ph}\gamma_r}{2}\mathcal{L}_{a^\dagger\sigma}\Big]\rho\,, \quad (11)$$

which are, like the decay terms, in the Lindblad form (Methods). The rate γ_ϕ accounts for the pure dephasing of the QE, while γ_r accounts for the phonon mediated coupling between the QD and the cavity. The case written is for negative detuning; the positive detuning counterpart exchanges the prefactors of the terms $\mathcal{L}(\sigma^\dagger a)$ and $\mathcal{L}(a^\dagger\sigma)$. The same procedure and analysis as detailed in the text can be carried out in the presence of these terms. We have considered them both independently in the regime of two-photon emission for the parameters of the text. The results are condensed in Fig. S7. Note that we did not look for the maximum purity of two-photon emission but considered how the optimum case without dephasing is affected by these two sources of decoherence. It is conceivable that the new terms are less harmful in other regimes (say at lower pumping) and that higher purities could be achieved in their presence. The figure shows that while decoherence does affect the purity of emission, the mechanism exhibits some robustness, with extended plateaus that set a goal for an optimum technology, while a fundamental demonstration appears within reach even in extremely noisy samples.

There is a clear physical reason why the mechanism is so resistant to dephasing. The main attribute to preserve is the bundle itself, that is to say, what is crucial is to maintain the ability of the system to release its energy exclusively in multiples of N. Now, the bundle emission takes place in a very small time window, that can be disrupted only for extremely large dephasing rates. The effect of dephasing for the rest of the time can have detrimental effects on other attributes such as the intensity of emission, but this is of little or no incidence for the usefulness of the device. This is the case for cavity feeding in the red-detuned configuration, where the transfer towards the dot can reduce the intensity of emission by blocking the QD. The excited QD releases its energy in a different solid angle and at a different frequency than the N-photon emission channel, so its spurious excitation is not damaging. As for the possibility to destroy a bundle by diverting one of its photons towards the QD rather than through the useful channel, since this is possible within the short time-window of emission only, this affects very little the purity. The scheme is even more resilient to pure dephasing, which is the most universal type of decoherence that one can expect to find in any system. The physical reason is also linked to the mechanism of bundles production, and is even less deleterious because it harms the QE alone with no concomitant penalty to the cavity. For most of the time, the QE undergoes Rabi oscillations driven by the laser. Their dephasing

is a cause of impediment for the buildup of the probability to have two photons, but this merely slows down the repetition rate. Once the state collapses, the whole cascade of photon emission unravels in the short time window, essentially shielded from dephasing of the QE. As a result, even with a considerable dephasing rate equal to the Rabi coupling rate, the mechanism still produces over 50% of two-photon bundles.

Now, in order to contrast Fig. S7 with the experimental state of the art: the semiconductor cavity QED literature reports largely varying values of dephasing rates, indicating that much room exists for optimization of the samples and reducing the sources of noise. Pure dephasing rates of $\gamma_\phi/g = 0.3$ have been estimated in the strong-coupling of a quantum dot to a microcavity at low temperature [24], and values as low as $\gamma_\phi/g = 0.025$ have been reported a few years later in similar semiconductor systems [7], with also a cavity feeding estimated at $\gamma_r/g = 0.025$. This shows that even the most noisy environment should already provide close to ideal two-photon emission. In atomic platforms, dephasing is so small that it is often neglected to fit the experimental results [29]. As for circuit QED, it has already reached the stage where dephasing is utterly negligible [30].

References

[1] Pearle, F. Wavefunction collapse and conservation laws. *Found. Phys.* **30**, 1145 (2000).

[2] Silverman, M. P. *Quantum superposition: counterintuitive consequences of coherence, entanglement, and interference* (Springer, 2008).

[3] Varcoe, B. T., Brattke, S., Weidinger, M. & Walther, H. Preparing pure photon number states of the radiation field. *Nature* **403** (2000).

[4] del Valle, E. Distilling one, two and entangled pairs of photons from a quantum dot with cavity QED effects and spectral filtering. *New J. Phys.* **15**, 025019 (2013).

[5] Greentree, A. D., Koch, J. & Larson, J. Fifty years of Jaynes–Cummings physics. *J. Phys. B: At. Mol. Opt. Phys.* **46**, 220201 (2013).

[6] Gies, C., Florian, M., Gartner, P. & Jahnke, F. The single quantum dot-laser: lasing and strong coupling in the high-excitation regime. *Opt. Express* **19**, 14370 (2011).

[7] Majumdar, A., Kim, E. D., Gong, Y., Bajcsy, M. & Vuckovic, J. Phonon mediated off-resonant quantum dot–cavity coupling under resonant excitation of the quantum dot. *Phys. Rev. B* **84**, 085309 (2011).

[8] Gonzalez-Tudela, A. *et al.* Effect of pure dephasing on the Jaynes-Cummings nonlinearities. *Opt. Express* **18**, 7002 (2010).

[9] Allen, L. & Eberly, J. H. *Optical Resonance and Two-Level Atoms* (Dover, 1987).

[10] Niemczyk, T. *et al.* Circuit quantum electrodynamics in the ultrastrong-coupling regime. *Nature Phys.* **6**, 772 (2010).

[11] Beaudoin, F., Gambetta, J. M. & Blais, A. Dissipation and ultrastrong coupling in circuit QED. *Phys. Rev. A* **84**, 043832 (2011).

[12] Forn-Díaz, P. *et al.* Observation of the Bloch-Siegert shift in a qubit-oscillator system in the ultrastrong coupling regime. *Phys. Rev. Lett.* **105**, 237001 (2010).

[13] Berlín, G. & Aliaga, J. Validity of the rotating wave approximation in the driven Jaynes–Cummings model. *J. Opt. B* **6**, 231 (2004).

[14] Hausinger, J. & Grifoni, M. Qubit-oscillator system under ultrastrong coupling and extreme driving. *Phys. Rev. A* **83**, 030301(R) (2011).

[15] Wallraff, A. *et al.* Strong coupling of a single photon to a superconducting qubit using circuit quantum electrodynamics. *Nature* **431**, 162 (2004).

[16] Fink, J. M. *et al.* Climbing the Jaynes–Cummings ladder and observing its $\sqrt{n}$ nonlinearity in a cavity QED system. *Nature* **454**, 315 (2008).

[17] Khitrova, G., Gibbs, H. M., Kira, M., Koch, S. W. & Scherer, A. Vacuum Rabi splitting in semiconductors. *Nat. Phys.* **2**, 81 (2006).

[18] Miller, R. *et al.* Trapped atoms in cavity QED: coupling quantized light and matter. *J. Phys. B.: At. Mol. Phys.* **38**, S551 (2005).

[19] Ridolfo, A., Leib, M., Savasta, S. & Hartmann, M. J. Photon blockade in the ultrastrong coupling regime. *Phys. Rev. Lett.* **109**, 193602 (2012).

[20] Bamba, M. & Ogawa, T. System-environment coupling derived by Maxwell's boundary conditions from the weak to the ultrastrong light-matter-coupling regime. *Phys. Rev. A* **88**, 013814 (2013).

[21] Schleich, P. *Quantum optics in phase space* (Wiley, 2011).

[22] Brown, K. R., Dani, K. M., Stamper-Kurn, D. M. & Whaley, K. B. Deterministic optical Fock-state generation. *Phys. Rev. B* **67**, 043818 (2003).

[23] Woolley, M. J., Lang, C., Eichler, C., Wallraff, A. & Blais, A. Signatures of Hong-Ou-Mandel interference at microwave frequencies. *New J. Phys.* **15**, 105025 (2013).

[24] Laucht, A. *et al.* Electrical control of spontaneous emission and strong coupling for a single quantum dot. *New J. Phys.* **11**, 023034 (2009).

[25] Hohenester, U. Cavity quantum electrodynamics with semiconductor quantum dots: Role of phonon-assisted cavity feeding. *Phys. Rev. B* **81**, 155303 (2010).

[26] Roy, C. & Hughes, S. Influence of electron–acoustic-phonon scattering on intensity power broadening in a coherently driven quantum-dot–cavity system. *Phys. Rev. X* **1**, 021009 (2011).

[27] Maragkou, M. *et al.* Bichromatic dressing of a quantum dot detected by a remote second quantum dot. *Phys. Rev. B* **88**, 075309 (2013).

[28] Florian, M., Gartner, P., Gies, C. & Jahnke, F. Phonon-mediated off-resonant coupling effects in semiconductor quantum-dot lasers. *New J. Phys.* **15**, 035019 (2013).

[29] Boca, A. *et al.* Observation of the vacuum Rabi spectrum for one trapped atom. *Phys. Rev. Lett.* **93**, 233603 (2004).

[30] Lang, C. *et al.* Correlations, indistinguishability and entanglement in Hong-Ou-Mandel experiments at microwave frequencies. *Nat. Phys.* **9**, 345 (2013).